Supporting Information

Comparing electrocatalytic and thermocatalytic conversion of nitrate on platinum-ruthenium alloys

Zixuan Wang, Evan M. Ortiz, Bryan R. Goldsmith*, Nirala Singh*

Department of Chemical Engineering, University of Michigan, Ann Arbor, Michigan 48109-2136, USA

Catalysis Science and Technology Institute, University of Michigan, Ann Arbor, Michigan 48109-2136, USA

Table of Contents

List of Figures

List of Tables

S1. Additional Synthesis and Characterization Results

A standard set of characterization experiments were performed on Pt/C, PtRu/C, $Pt_{75}Ru_{25}$/C, and Ru/C. Due to the instability of Ru/C for electrochemical experiments for comparison, this material was omitted from kinetic measurements and major results presented. **Fig. S1** shows the results from thermal gravimetric analysis (TGA) of the Vulcan carbon supported catalysts. Both the Pt/C and PtRu/C showed total metal loading around 30 wt%, as expected. The synthesized $Pt_{75}Ru_{25}$/C had 5 wt% lower loading than targeted, indicating that not all the precursor was deposited on the supported during synthesis. The manufacturing company claimed a 20 wt% loading for Ru/C, but the TGA results show loadings closer to 30 wt%.

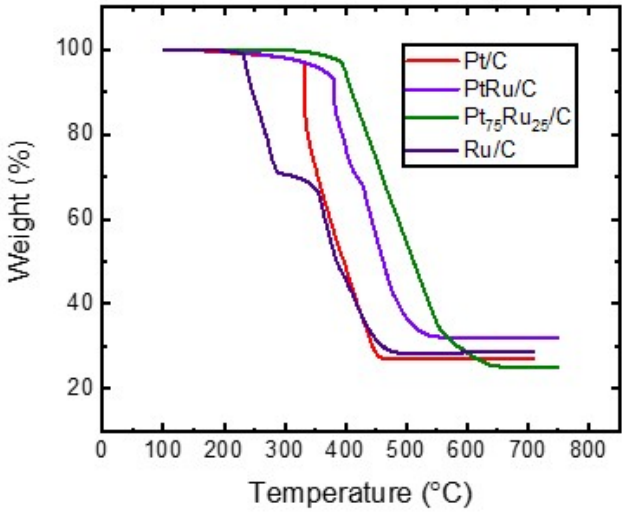

Figure S1. Thermal gravimetric analysis data of the Vulcan carbon-based catalysts in air. Treatments were conducted by first degassing the samples in He at 100 °C before ramping at 10 °C/min.

X-ray diffraction (XRD) spectra for Pt_xRu_y/C catalysts and the corresponding Pt and Ru powder diffraction files are provided in **Fig. S2**. Similar to the trends observed in our prior work on Pt_xRu_y/C,[3] increasing Ru composition in the material increases the 2θ angle of the Pt peaks. There are no separate Pt and Ru peaks present in the alloys, indicating no phase segregation in the material.

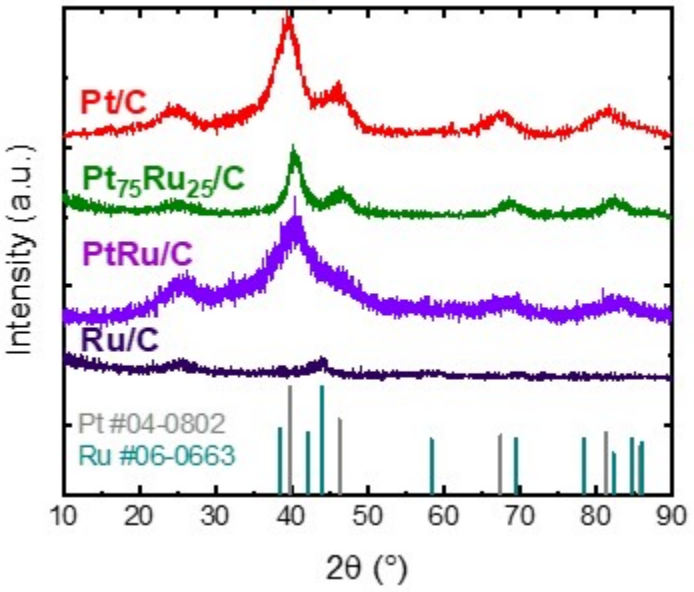

Figure S2. X-ray diffraction spectra of Pt_xRu_y/C catalysts with Cu Kα radiation and a Ni filter (λ = 1.5418 Å) from 10° to 90° 2θ range. Crystallite sizes were estimated by applying the Scherrer equation and the Pt and Ru peaks are referenced to #04-0802 and #06-0663, respectively.

The crystallite sizes and weight loading of the catalysts were calculated by applying the Scherrer equation (**Table S1**). The different catalysts have roughly the same average particle sizes. Additionally, we confirm that the particle size of $Pt_{75}Ru_{25}$/C matched previously synthesized materials.[3]

Table S1. Crystallite sizes and metal weight percent loading for platinum-ruthenium catalysts. The crystallite sizes are calculated from the Scherrer equation while the metal weight loadings are obtained from TGA experiments. The error is calculated from the deviation from each individual metal peaks in the XRD spectra.

Catalysts	Crystallite Size (nm)	Weight Loading (%)
Pt/C	2.6 ± 0.6	27.3
PtRu/C	2.4 ± 0.3	32.2
$Pt_{75}Ru_{25}$/C	3.7 ± 1.0	25.1
Ru/C	2.9 ± 0.5	28.7

Scanning electron microscopy (SEM) images and elemental analysis from energy dispersive spectroscopy (EDX) are shown in **Fig. S3** and **Fig. S4**, respectively. EDX analysis reveal that the metal nanoparticles are dispersed on the surface of the support and confirms that the Ru at% increases as the Ru content in the alloy increases. Also, the at% of the metal averaged over three different areas in the EDX analysis shows that the surface composition of metals is similar to the target composition from synthesis.

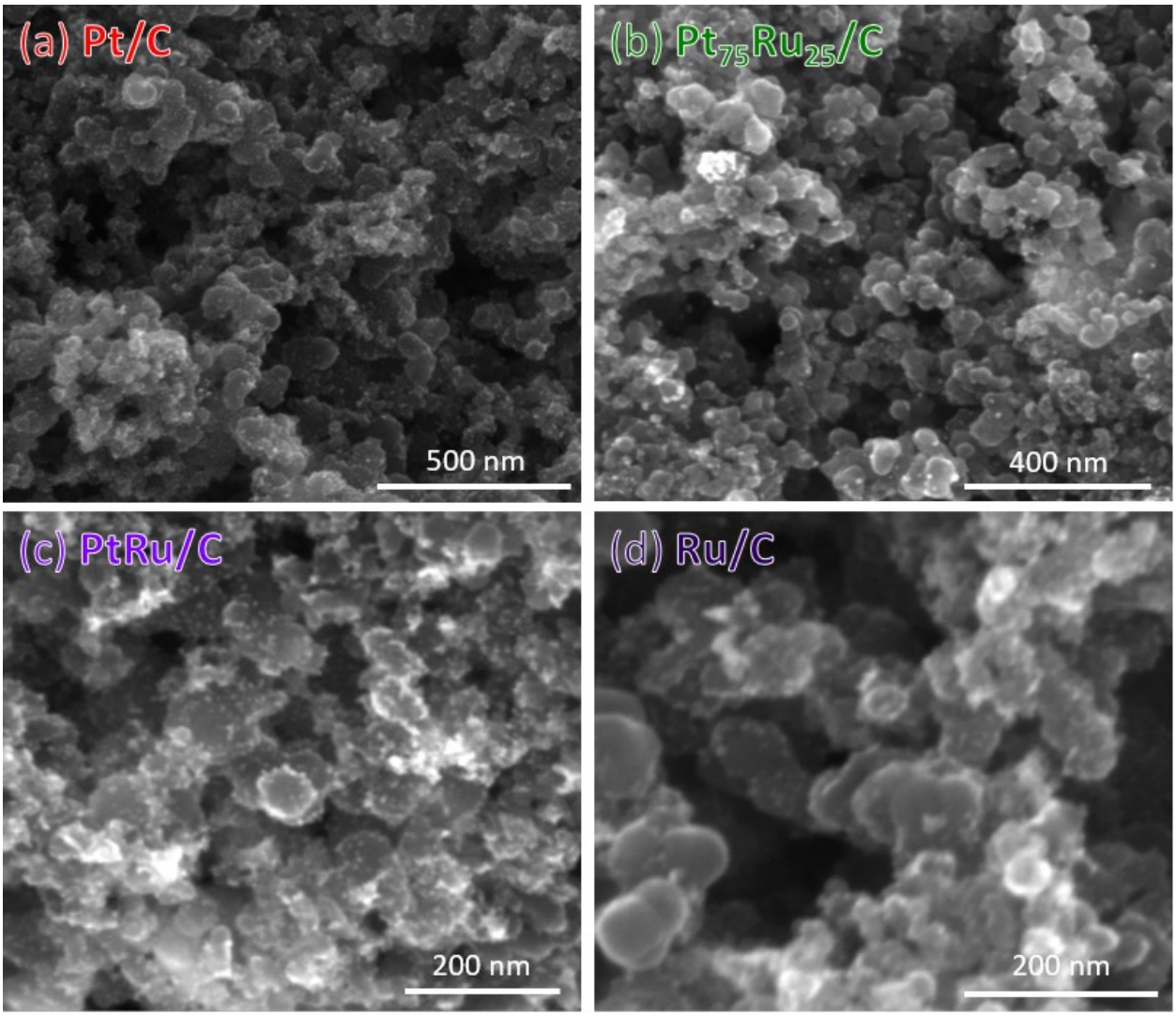

Figure S3. Scanning electron microscopy images of **(a)** Pt/C, **(b)** $Pt_{75}Ru_{25}$/C, **(c)** PtRu/C, and **(d)** Ru/C. The accelerating voltage is set at 10 kV with 5 mm working distance.

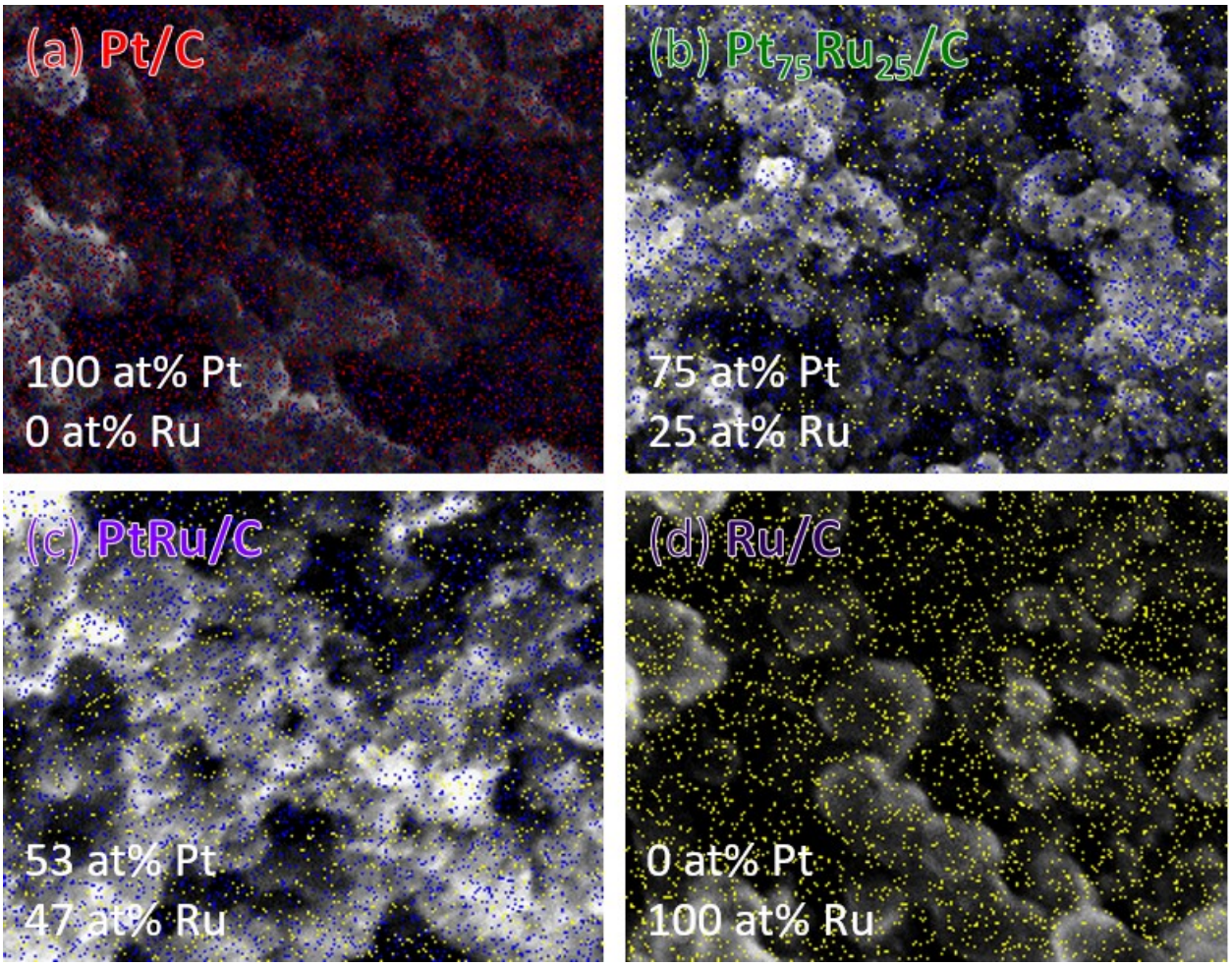

Figure S4. Overlay of elemental analysis from energy-dispersive X-ray spectroscopy on SEM images for **(a)** Pt/C, **(b)** $Pt_{75}Ru_{25}$/C, **(c)** PtRu/C, and **(d)** Ru/C. Color legend: carbon = red; platinum = blue; ruthenium = yellow.

S2. Additional Thermocatalytic Experimental Results

To ensure that no mass diffusion limitations occurred throughout TNO_3RR experiments, the ammonia production rate throughout the course of the reaction was measured for PtRu/C at three different stir rates (**Fig. S5**). As the catalysts are non-porous (and thus there are no internal diffusion limitations), these results indicate a lack of transport limitations here.

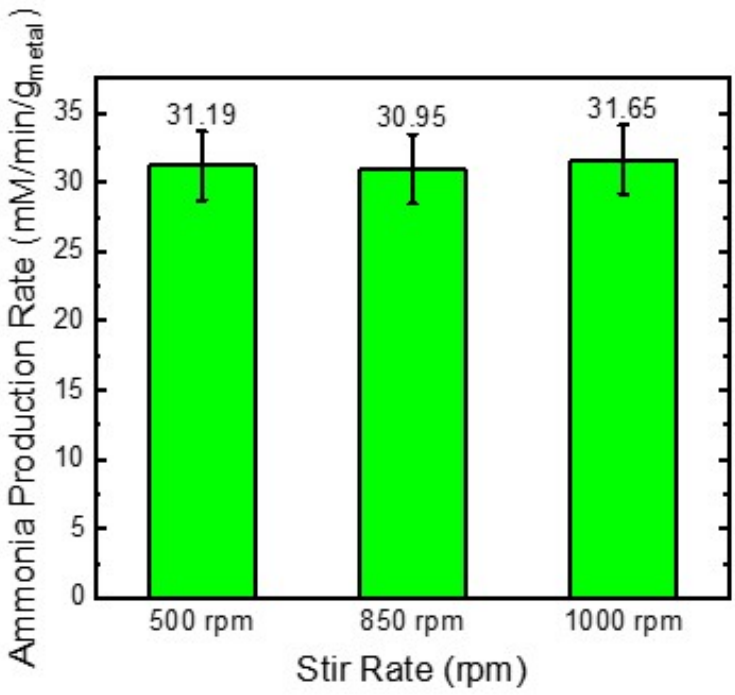

Figure S5. Measured ammonia production rate for TNO_3RR on PtRu/C at pH 2 and 0.01 M $NaNO_3$ at stir rates from 500–1000 rpm. Average ammonia production rates are written inset. Experiments were performed at room temperature (23.3 °C) and the partial pressure of H_2 was 0.5 atm.

Additional baseline experiments were performed to ensure that the catalytic effects observed are due to the metal alloy. **Fig. S6a** and **Fig. S6b** display the nitrate and product (i.e., ammonia, nitrite) concentrations over the course of a standard 90 min reaction using no catalyst and Vulcan carbon, respectively. Without the presence of metals on the Vulcan carbon support, no catalytic activity is recorded. The miniscule amount of ammonia shown in these figures (~0.02 mM) is subtracted as a baseline for analysis. A known concentration of ammonia is recorded over the course of the reaction in **Fig. S6c**. The consistent level of ammonia concentration indicates that aqueous ammonia does not evaporate with continuous H_2 bubbling through the system.

For TNO_3RR measurements for Pt/C, there was no observed nitrate conversion and ammonia production activity. To ensure that this result is due to a catalytic effect rather than experimental design issue, we increased the amount of Pt/C in the reactor from 10 mg to 50 mg. **Fig. S6d** shows no significant change in catalytic activity with increasing the amount of catalyst in the reactor. For comparison, the nitrate concentration for PtRu/C is provided, where a drastic drop in nitrate is recorded over the course of 90 min.

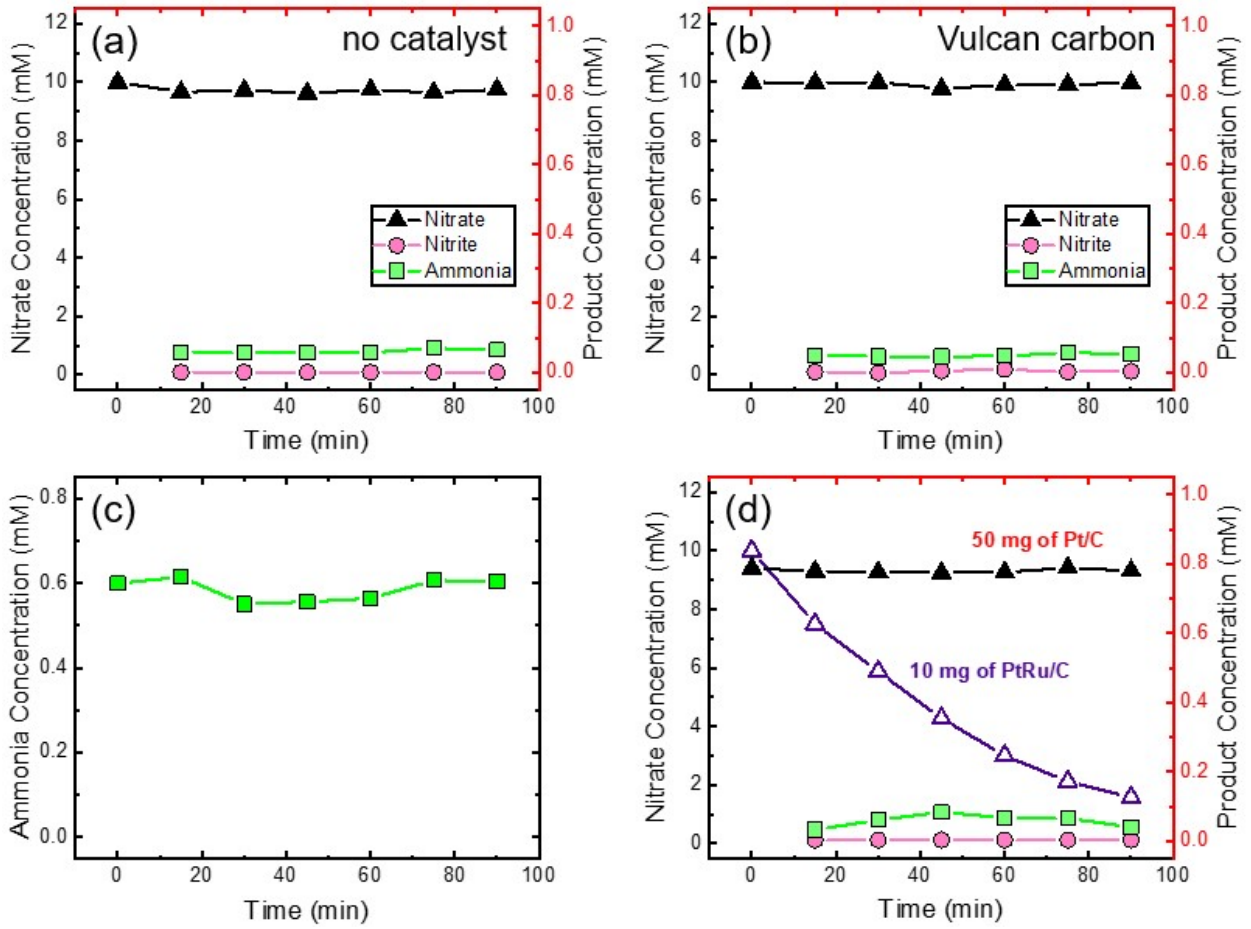

Figure S6. Initial baseline measurements for TNO_3RR measurements. Nitrate, nitrite, and ammonia concentration under reaction conditions (pH 2, 0.01 M $NaNO_3$) **(a)** with no added catalyst and **(b)** with Vulcan carbon support only. **(c)** Known concentration of ammonia over 90 min of reaction to ensure no ammonia evaporation from H_2 bubbling into the system. **(d)** Comparison of the nitrate concentration of reaction with 50 mg of Pt/C and 10 mg of PtRu/C. Ammonia and nitrite concentrations throughout the reaction from Pt/C. Color legend: nitrate = black, ammonia = green, nitrite = pink.

S3. Additional Kinetic Modeling Procedures and Results

S.3.1 Kinetic Model Procedure

Assuming ENO_3RR follows a Langmuir-Hinshelwood model, both a single site model (SSM) and multisite model (MSM) were considered to model the reaction. SSM assumes a homogeneous electrode surface, the rate r can be derived as shown is **Eq. S1** by inserting expressions for the coverages into **Eq. 1**. Both nitrate and H^+ adsorb onto this single site and competitively inhibit the other species. The adsorption equilibrium constants K_N and K_H refer to the adsorption of nitrate and H^+, respectively; C_i refers to the bulk concentration of species i; k_{SSM} denotes the rate constant of the surface reaction between adsorbed nitrate and hydrogen for the SSM.

$$r = k_{SSM}\frac{K_N K_H C_N C_H}{(1 + K_N C_N + K_H C_H)^2}\ [M\,s^{-1}\,m^{-2}] \quad \text{(S1)}$$

If TNO_3RR follows a surface reaction RDS, it will obey the same rate equation.

The main assumptions of the proposed multisite kinetic model (MSM) are as follows: 1) There are two adsorption sites on the catalyst surface, $*_1$,$*_2$; 2) The reaction only occurs between NO_3*_1 and $H*_2$ and thus each species competitively inhibits the other on the opposite site. Adsorption equilibrium constants K_1, K_2, K_3, K_4, refer to **Eqs. S2**–**5**, respectively.

$$NO_3^- + *_1 \rightleftharpoons NO_3^{*1} + e^- \tag{S2}$$

$$NO_3^- + *_2 \rightleftharpoons NO_3^{*2} + e^- \tag{S3}$$

$$H^+ + *_1 + e^- \rightleftharpoons H^{*1} \tag{S4}$$

$$H^+ + *_2 + e^- \rightleftharpoons H^{*2} \tag{S5}$$

The rate determining step is seen in **Eq. S6**, resulting in the corresponding rate law shown in **Eq. S7**.

$$NO_3^{*1} + H^{*2} \rightarrow NO_2^* + OH^* \tag{S6}$$

$$r = k_{MSM}\theta_{N^{*1}}\theta_{H^{*2}} \tag{S7}$$

In **Eq. S7**, $\theta_{i^{*j}}$ refers to the surface coverage of the species i on site j. From these assumptions, and assuming quasi-equilibrium in the adsorption reactions in **Eqs. S2–S5**, a rate law (**Eq. S8**) is derived relating reaction rate with bulk concentration of nitrate (C_N) and H^+ (C_H), a constant of proportionality k_{MSM} *[M s^{-1} m^{-2}]*, and using a site balance in **Eq S9**.

$$r = k_{MSM}\frac{C_N C_H}{K_1 K_4\left(\frac{C_N}{K_1} + \frac{C_H}{K_3} + 1\right)\left(\frac{C_N}{K_2} + \frac{C_H}{K_4} + 1\right)} \tag{S8}$$

$$1 = \theta_{N^{*1}} + \theta_{H^{*1}} + \theta_{*1} = \theta_{N^{*2}} + \theta_{H^{*2}} + \theta_{*2} \tag{S9}$$

θ_{*1} and θ_{*2} are the coverage of open sites on site 1 and 2, respectively. This MSM rate law is compared to that of the SSM for accuracy in predicting the nitrate reduction reaction rate. A nonlinear least-square regression was performed on MATLAB version R2020b, relating current density to concentration of H^+. The SSM can be reduced to a two-parameter fit (**Eqs. S10, S11**), and the MSM to a three-parameter fit (**Eqs. S12, S13**). The independent variable, x, may refer to C_H, or 10^{-pH} depending on context.

$$r = \frac{\alpha x}{(\beta + x)^2} \tag{S10}$$

$$\alpha = k_{SSM}\frac{K_N C_N}{K_H}\ [M^2\ s^{-1}\ m^{-2}],\quad \beta = \frac{1}{K_H} + \frac{K_N C_H}{K_H}\ [M] \tag{S11}$$

$$r = \frac{Ax}{(x + B)(x + C)} \tag{S12}$$

$$A = k_{MSM}\frac{C_N K_3}{K_1}\ [M^2\ s^{-1}\ m^{-2}],\ B = \frac{C_N K_3}{K_1} + K_4\ [M],\quad C = \frac{C_N K_4}{K_2} + K_4\ [M] \tag{S13}$$

S.3.2 Kinetic Model Results

When fitting the LH models to nitrate concentration and experimental data, the *B* and *C* fit parameters become equivalent, rendering the MSM mathematically identical to the SSM. The data in **Fig. S7** shows the fit of this LH model to the experimental ENO_3RR activity at pH 1 and 7 for the considered catalysts. The nitrate concentration has little effect on the activity of Pt/C. The rate of reaction on Pt_xRu_y/C at pH 1 and pH 7 has a positive order with respect to nitrate concentration until 0.5 M, where it becomes negative order. $Pt_{75}Ru_{25}/C$ in pH 7 is the exception to this trend. The model qualitatively agrees with the experimental data, and helps to explain that increasing in nitrate concentration is associated with increasing nitrate reduction activity up until concentrations between 0.2–0.4 M NO_3^- as the nitrate coverage increases, whereas at higher nitrate coverages the surface sites are blocked by nitrate and cause the rate to decrease.

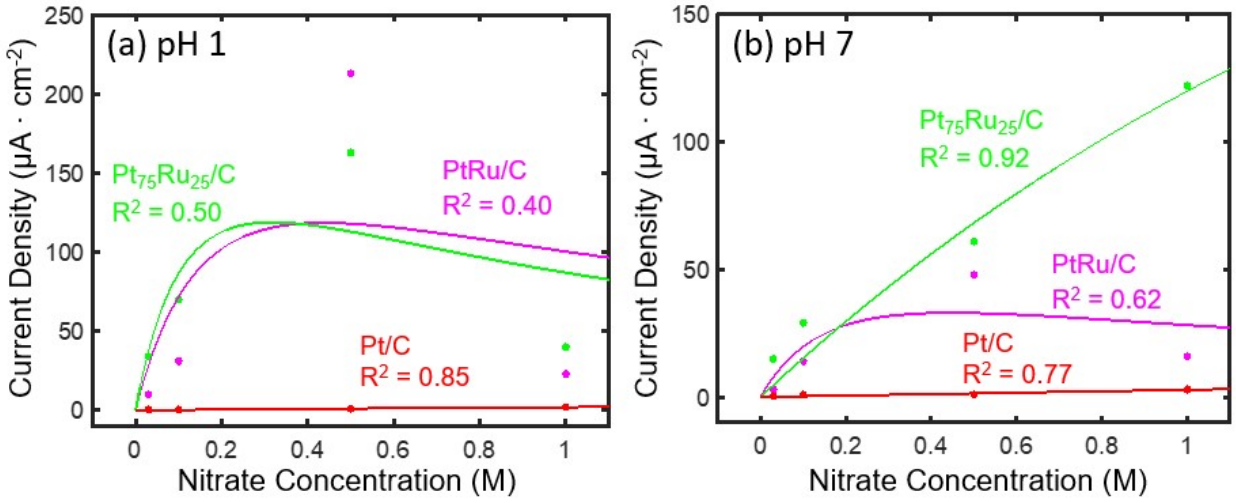

Figure S7. Langmuir-Hinshelwood model of ENO_3RR activity for Pt_xRu_y/C catalysts as a function of nitrate concentration at **(a)** pH 1 and **(b)** pH 7. All experimental data points are collected at 0.1 V vs. RHE. Coefficient of determination R^2 is written inset.

Initially, both the SSM and MSM were fit to a pH range of 0–7 to describe the C_H effect on rate (**Fig. S8a**). Similar to fitting the data to nitrate concentration, B and C fit parameters become equivalent, rendering the MSM mathematically identical to the SSM. In this analysis, pH 10 data was omitted due to potential oxide formation skewing the measured reduction currents. Results of the fitting show negative R^2 values, which indicate that a simple Langmuir-Hinshelwood model does not capture all the pH effects on nitrate reduction activity. Previous experiments show that catalyst activity is dependent on C_H at pH < 4.[4,5] Thus, additional fittings were conducted between pH 0–4 for the SSM (**Fig. S8b**) and MSM (**Fig. S8c**). Although there are only three data points for each catalyst at this pH range, the MSM shows a superior fit over the SSM fit.

The kinetic models explored are simplistic and only capture direct effects of C_H and C_N, and thus cannot provide a comprehensive understanding for the effect of pH on reaction rate. For example, pH affects the adsorption equilibria of both nitrate and protons while the model assumes these equilibria to be fixed. Future works should focus on improving these models by incorporating expressions that account for pH effects on the system.

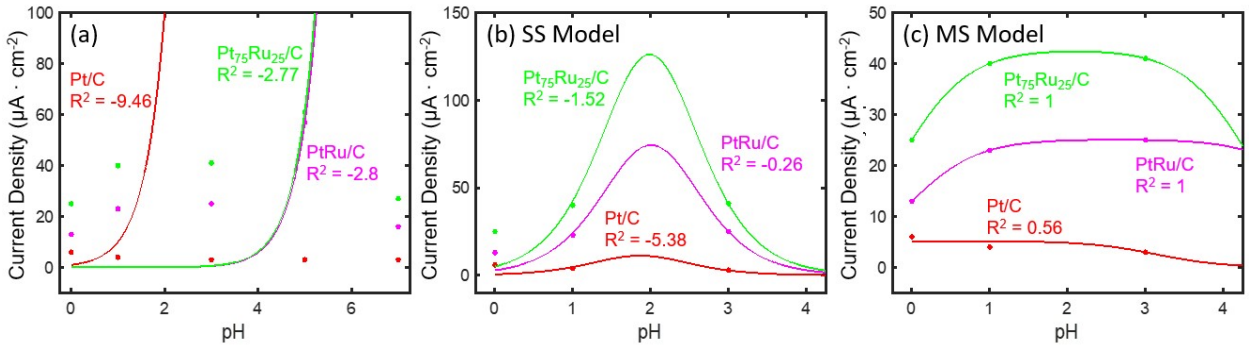

Figure S8. SSM and MSM Langmuir-Hinshelwood models of ENO_3RR activity for Pt_xRu_y/C catalysts as a function of pH. **(a)** LH fitting for data collected between pH 0–7. **(b)** SSM for pH 0–3, and **(c)** MSM for pH 0–3. All experimental data points are collected at 0.1 V vs. RHE.

S4. Additional Electrocatalytic Experimental Results

The FE of PtRu/C towards NH_3 at pH 1 and pH 7 are shown in **Fig. S9**. The reactions were performed at 0.1 V vs. RHE for at least 6 hrs. The FE reaches ~ 93% at pH 1 after 5.5 hrs, whereas the FE reaches ~54% at pH 7 after 3 hrs. The increase in the measured FE over time can be attributed to many factors. Because the measurements are performed in a batch reactor on a porous carbon felt, diffusion limitations may delay the transport of the products to the bulk solution. It is also possible that some intermediates are forming on the surface of the felt but reacting slowing, which results in high FE towards ammonia once the intermediates react. The reported FE in the main text is the averaged last four timepoints in each experiment.

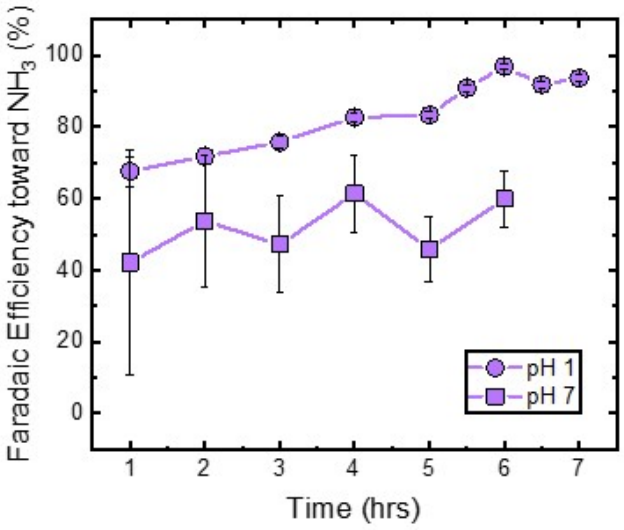

Figure S9. Comparison between the faradaic efficiency of 10 mg of PtRu/C deposited on carbon felts in pH 1 (0.1 M HNO_3) and pH 7 (0.2 M sodium phosphate + 0.1 citric acid) electrolyte solution. Both experiments are conducted with 0.1 M nitrate at 0.1 V vs. RHE for at least 6 hrs.

With the current data that we have collected, we performed a Tafel analysis for the pH effect for PtRu/C (**Fig. S10**). The Tafel analysis in **Fig. S10a** allowed us to extract Tafel slopes for the different pH values and electrocatalysts (**Fig. S10b**). There was not a clear trend with pH, but the Tafel slopes were different depending on the pH value. The Tafel slopes were similar for each electrocatalyst at a given pH. The Tafel slope differences may be representative of mechanistic changes or a change in the rate-determining step as pH is varied, and future studies that include a wider range of applied potentials at specific pH may yield greater insight into the reaction mechanism.

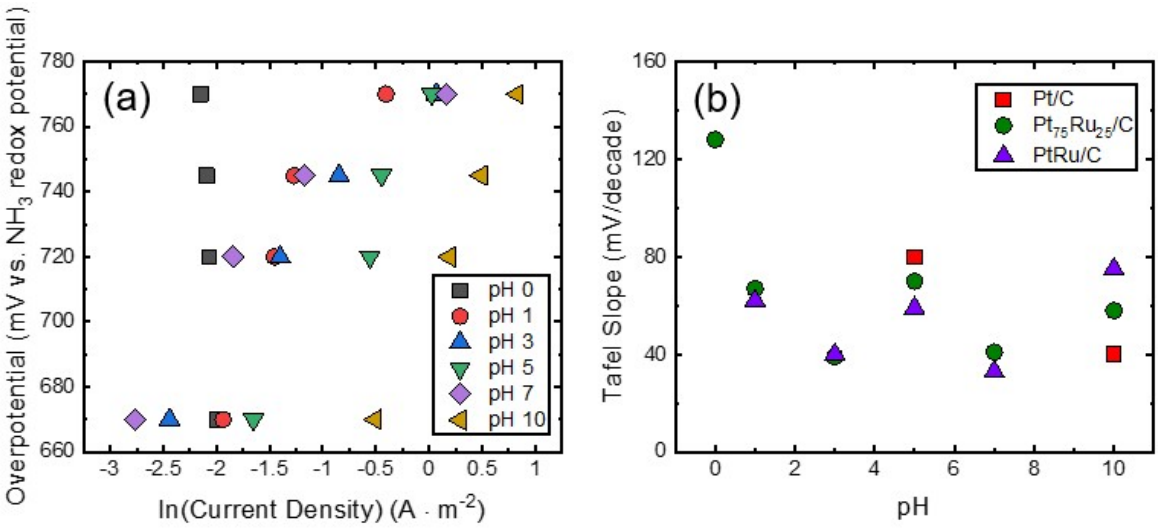

Figure S10. (a) Tafel analysis of PtRu/C for pH 0 – 10. **(b)** Reported Tafel slopes for Pt/C, $Pt_{75}Ru_{25}$/C, and PtRu/C for pH 0 – 10. The electrolyte solution at each pH is: pH 0 – 1 M H_2SO_4, pH 1 – 0.1 M H_2SO_4,

pH 3 – 0.1 M sodium citrate + 0.1 M citric acid, pH 5 – 0.2 M sodium acetate + 0.2 M acetic acid, pH 7 – 0.2 M sodium phosphate + 0.1 M citric acid, pH 10 – 0.1 M sodium carbonate + 0.1 M sodium bicarbonate.

To obtain further insights on the effect of pH on the activity of the PtRu/C catalyst, we examined the absolute current densities in **Fig. 4** as a function of the absolute potential in SHE. The results of this analysis are displayed in **Fig. S11** and demonstrate the significant difference in the electrode potential when operating at different pH values, even if the voltage vs. RHE is the same. This indicates work to understand how the voltage vs. SHE influences the catalyst structure or adsorption of cations other than protons or anions such as nitrate is needed to deconvolute the effect of pH.

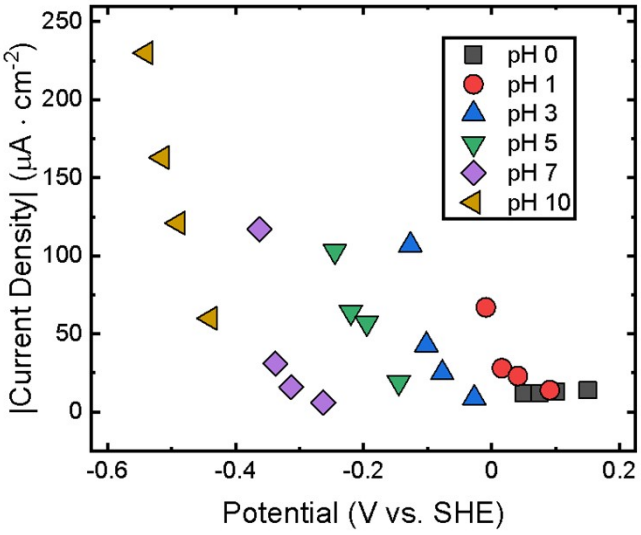

Figure S11. Comparison between the faradaic efficiency of 10 mg of PtRu/C deposited on carbon felts in pH 1 (0.1 M HNO_3) and pH 7 (0.2 M sodium phosphate + 0.1 citric acid) electrolyte solution. Both experiments are conducted with 0.1 M nitrate at 0.1 V vs. RHE for at least 6 hrs.

To further understand the change in the catalyst over the course of an electrochemical experiment, we use XPS surface characterization on PtRu/C deposited on a glassy carbon electrode before and after an 8-hour steady-state measurement at 0.1 V vs. RHE in pH 10 solution. After normalization, the spectra from **Fig. S12** show that both surface Pt and Ru content marginally decreased after an extended run. The low intensity of the peaks from the measurements also makes it difficult to deconvolute Ru 3p for the oxidation states.

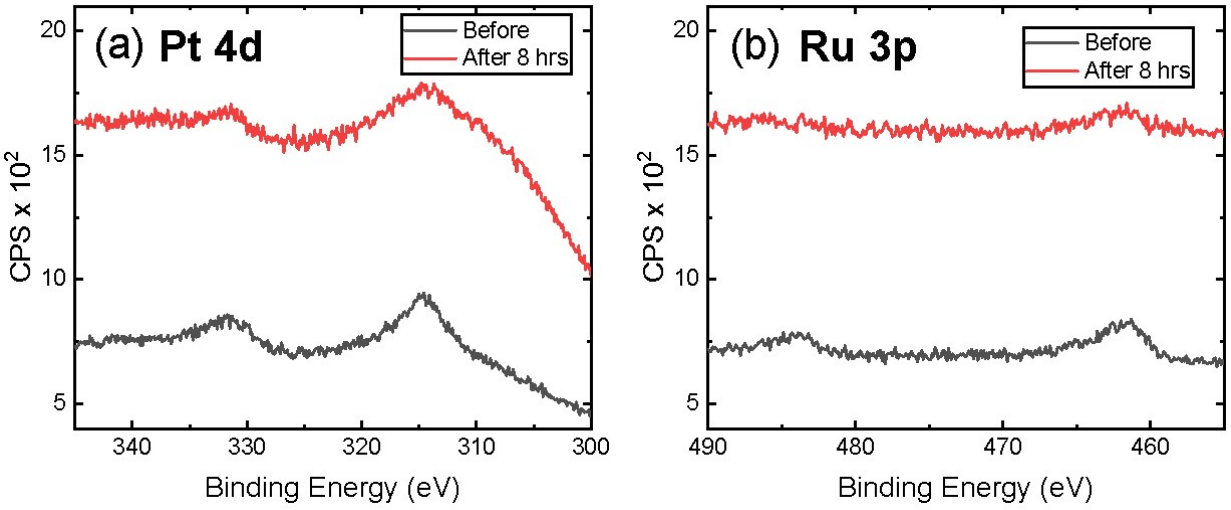

Figure S12. (a) Pt 4d scan of the PtRu/C catalyst deposited onto a glassy carbon disk before and after operation at 0.1 V vs. RHE in sodium carbonate/sodium bicarbonate (pH = 10) for 8 hours. **(b)** Ru 3p scan for the same catalysts.

For all the ENO_3RR measurements in different pH, different buffer solutions were prepared to ensure that the pH of the solution remains constant throughout the reaction. However, the ionic strength of the solution can also influence the reduction currents.[4,5] **Fig. S13** displays the calculated ionic strength of all the buffer solutions prepared for the pH experiments, and shows a large variation between 0.25–2.5 M for different electrolytes. However, the pH trends do not match the ionic strengths of the solution, implying that other effects, such as hydrogen equilibrium potential,[6] the point of zero free charge (pzfc),[7–9] and water orientation and interfacial solvent reorganization energy,[10–12] may also influence the current measurements with varying pH.

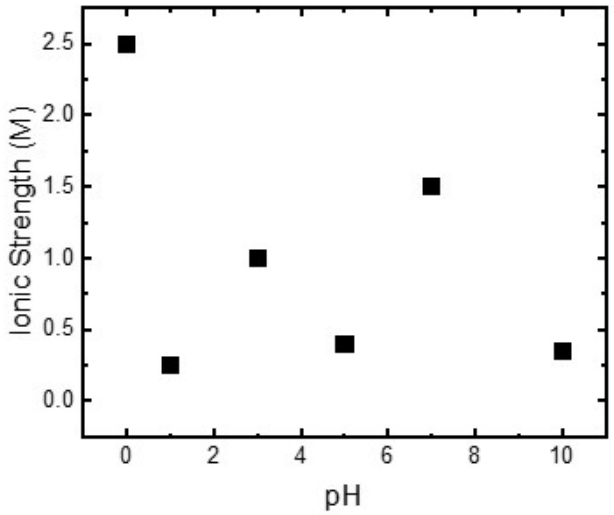

Figure S13. Calculated ionic strength of all pH solutions for ENO_3RR experiments. The electrolyte solution at each pH is listed: pH 0: 1 M H_2SO_4, pH 1: 0.1 M H_2SO_4, pH 3: 0.1 M sodium citrate + 0.1 M citric acid, pH 5: 0.2 M sodium acetate + 0.2 M acetic acid, pH 7: 0.2 M sodium phosphate + 0.1 M citric acid, pH 10: 0.1 M sodium carbonate + 0.1 M sodium bicarbonate.

S5. Net Changes in pH During Reaction

The balanced full-cell nitrate to ammonia reaction for ENO_3RR is:

$NO_{3(aq)}^{-} + 9H^{+} + 8e^{-} \rightleftharpoons NH_{3(aq)} + 3H_2O_{(l)}; E^o = 0.82\ V\ vs.\ RHE$

$4H_2O_{(l)} \rightleftharpoons 2O_{2(g)} + 8e^{-} + 8H^{+}; E^o = 1.23\ V\ vs.\ RHE$

Here we assume oxygen evolution is the anodic reaction. The net reaction is:

$NO_{3(aq)}^{-} + H^{+} + H_2O_{(l)} \rightleftharpoons NH_{3(aq)} + 2O_{2(g)}$

For TNO_3RR, if the hydrogen is produced from water electrolysis the reaction is:

$8e^{-} + 8H^{+} \rightleftharpoons 4H_{2(g)}; E^o = 0\ V\ vs.\ RHE$

$4H_2O_{(l)} \rightleftharpoons 2O_{2(g)} + 8e^{-} + 8H^{+}; E^o = 1.23\ V\ vs.\ RHE$

The TNO_3RR using this hydrogen is:

$H^{+} + NO_{3(aq)}^{-} + 4H_{2(g)} \rightleftharpoons NH_{3(aq)} + 3H_2O_{(l)}$

Thus, the net reaction is the same as ENO_3RR if H_2 comes from water electrolysis:

$NO_{3(aq)}^{-} + H^{+} + H_2O_{(l)} \rightleftharpoons NH_{3(aq)} + 2O_{2(g)}$

Therefore, in both cases one net proton would be consumed per ammonia produced, requiring a balancing to maintain a constant pH. Although more than one proton is required for ENO_3RR half-cell reaction, all but one proton is provided from the anodic reaction, which in a commercial system would be via a proton conducting membrane. Without a sufficiently conductive or selective membrane, a local pH gradient may build up at the cathode compartment in a commercial system, which should be considered in future studies.

References

(1) Baturina, O. A.; Aubuchon, S. R.; Wynne, K. J. Thermal Stability in Air of Pt/C Catalysts and PEM Fuel Cell Catalyst Layers. *Chem. Mater.* **2006**, *18* (6), 1498–1504. https://doi.org/10.1021/cm052660e.

(2) Pinchuk, O. A.; Aubuchon, S. R.; Marks, C.; Dominey, R.; Dundar, F.; Deniz, O. F.; Ata, A.; Wynne, K. J. Thermally Pretreated 46% Pt/Vulcan XC72: Characterisation by TGA/DSC/TEM and Cyclic Voltammetry. *Fuel Cells* **2009**, *9* (5), 554–561. https://doi.org/10.1002/fuce.200800183.

(3) Wang, Z.; Young, S. D.; Goldsmith, B. R.; Singh, N. Increasing Electrocatalytic Nitrate Reduction Activity by Controlling Adsorption through PtRu Alloying. *Journal of Catalysis* **2021**, *395*, 143–154. https://doi.org/10.1016/j.jcat.2020.12.031.

(4) Dortsiou, M.; Katsounaros, I.; Polatides, C.; Kyriacou, G. Influence of the Electrode and the PH on the Rate and the Product Distribution of the Electrochemical Removal of Nitrate. *Environmental Technology* **2013**, *34* (3), 373–381. https://doi.org/10.1080/09593330.2012.696722.

(5) Yang, J.; Sebastian, P.; Duca, M.; Hoogenboom, T.; M. Koper, M. T. PH Dependence of the Electroreduction of Nitrate on Rh and Pt Polycrystalline Electrodes. *Chemical Communications* **2014**, *50* (17), 2148–2151. https://doi.org/10.1039/C3CC49224A.

(6) Jerkiewicz, G. Standard and Reversible Hydrogen Electrodes: Theory, Design, Operation, and Applications. *ACS Catal.* **2020**, *10* (15), 8409–8417. https://doi.org/10.1021/acscatal.0c02046.

(7) Silva, F.; Sottomayor, M. J.; Hamelin, A. The Temperature Coefficient of the Potential of Zero Charge of the Gold Single-Crystal Electrode/Aqueous Solution Interface: Possible

Relevance to Gold-Water Interactions. *Journal of Electroanalytical Chemistry and Interfacial Electrochemistry* **1990**, *294* (1), 239–251. https://doi.org/10.1016/0022-0728(90)87148-D.

(8) Rizo, R.; Sitta, E.; Herrero, E.; Climent, V.; Feliu, J. M. Towards the Understanding of the Interfacial PH Scale at Pt(111) Electrodes. *Electrochimica Acta* **2015**, *162*, 138–145. https://doi.org/10.1016/j.electacta.2015.01.069.

(9) Ganassin, A.; Sebastián, P.; Climent, V.; Schuhmann, W.; Bandarenka, A. S.; Feliu, J. On the PH Dependence of the Potential of Maximum Entropy of Ir(111) Electrodes. *Scientific Reports* **2017**, *7* (1), 1246. https://doi.org/10.1038/s41598-017-01295-1.

(10) García-Aráez, N.; Climent, V.; Feliu, J. M. Evidence of Water Reorientation on Model Electrocatalytic Surfaces from Nanosecond-Laser-Pulsed Experiments. *J. Am. Chem. Soc.* **2008**, *130* (12), 3824–3833. https://doi.org/10.1021/ja0761481.

(11) Ledezma-Yanez, I.; Wallace, W. D. Z.; Sebastián-Pascual, P.; Climent, V.; Feliu, J. M.; Koper, M. T. M. Interfacial Water Reorganization as a PH-Dependent Descriptor of the Hydrogen Evolution Rate on Platinum Electrodes. *Nature Energy* **2017**, *2* (4), 1–7. https://doi.org/10.1038/nenergy.2017.31.

(12) Sarabia, F. J.; Sebastián-Pascual, P.; Koper, M. T. M.; Climent, V.; Feliu, J. M. Effect of the Interfacial Water Structure on the Hydrogen Evolution Reaction on Pt(111) Modified with Different Nickel Hydroxide Coverages in Alkaline Media. *ACS Appl. Mater. Interfaces* **2019**, *11* (1), 613–623. https://doi.org/10.1021/acsami.8b15003.